AEM
Journals.ASM.org

Arsenic Bioremediation by Biogenic Iron Oxides and Sulfides

Enoma O. Omoregie,[a,b,c]* Raoul-Marie Couture,[d,e]* Philippe Van Cappellen,[d,e] Claire L. Corkhill,[a,f] John M. Charnock,[a] David A. Polya,[a] David Vaughan,[a] Karolien Vanbroekhoven,[c] Jonathan R. Lloyd[a]

Williamson Research Centre for Molecular Environmental Science and School of Earth, Atmospheric and Environmental Sciences, University of Manchester, Manchester, United Kingdom[a]; Department of Earth Sciences, Utrecht University, Utrecht, Netherlands[b]; Flemish Institute for Technological Research, Mol, Belgium[c]; School of Earth and Atmospheric Sciences, Georgia Institute of Technology, Atlanta, Georgia, USA[d]; Earth and Environmental Sciences, University of Waterloo, Waterloo, Ontario, Canada[e]; Department of Materials Science and Engineering, The University of Sheffield, Sheffield, United Kingdom[f]

Microcosms containing sediment from an aquifer in Cambodia with naturally elevated levels of arsenic in the associated groundwater were used to evaluate the effectiveness of microbially mediated production of iron minerals for *in situ* As remediation. The microcosms were first incubated without amendments for 28 days, and the release of As and other geogenic chemicals from the sediments into the aqueous phase was monitored. Nitrate or a mixture of sulfate and lactate was then added to stimulate biological Fe(II) oxidation or sulfate reduction, respectively. Without treatment, soluble As concentrations reached 3.9 ± 0.9 μM at the end of the 143-day experiment. However, in the nitrate- and sulfate-plus-lactate-amended microcosms, soluble As levels decreased to 0.01 and 0.41 ± 0.13 μM, respectively, by the end of the experiment. Analyses using a range of biogeochemical and mineralogical tools indicated that sorption onto freshly formed hydrous ferric oxide (HFO) and iron sulfide mineral phases are the likely mechanisms for As removal in the respective treatments. Incorporation of the experimental results into a one-dimensional transport-reaction model suggests that, under conditions representative of the Cambodian aquifer, the *in situ* precipitation of HFO would be effective in bringing groundwater into compliance with the World Health Organization (WHO) provisional guideline value for As (10 ppb or 0.13 μM), although soluble Mn release accompanying microbial Fe(II) oxidation presents a potential health concern. In contrast, production of biogenic iron sulfide minerals would not remediate the groundwater As concentration below the recommended WHO limit.

The release of arsenic from sediments into groundwater is a global problem that has been highlighted in numerous studies over the past decade (1, 2). The consumption of water containing elevated As levels has been linked to numerous types of cancers, including kidney, lung, and bladder cancer (3), as well as various attritional diseases (4). The World Health Organization (WHO) provisional guide value for the maximum concentration of As in drinking water is 10 ppb, or 0.13 μM (5). However, tens of millions of people worldwide are exposed to arsenic levels in excess of 10 ppb (2, 6). In Southeast Asia alone, the number may be over 40 million people (7). The microbially mediated dissolution of iron- and arsenic-bearing minerals, leading to the release of As into groundwater (8), is widely believed to be one of the major causes of As groundwater contamination in the region.

Despite the global occurrence of groundwater As concentrations exceeding safe drinking water standards and the broad range of proposed As remediation technologies based on volatilization, precipitation, sorption, and ion exchange, the large-scale implementation of *in situ* attenuation and remediation schemes remains elusive. Arsenic remediation through coprecipitation with biogenically formed Fe(III) oxyhydroxides/oxides (also termed hydrous ferric oxides [HFO]) or iron sulfides represents one of the more attractive approaches, because it offers simple and potentially cost-effective solutions.

The sorption of As and other metalloids and metals by HFO has been studied extensively (9, 10). A number of experimental studies have investigated the potential remediation of As based on its affinity for HFO (11, 12). Biologically, HFO is produced by the transfer of electrons from Fe(II) to a variety of electron acceptors, including oxygen and nitrate (13, 14). A variety of organisms present in freshwater systems have been shown to be able to couple Fe(II) oxidation to the reduction of nitrate (15). The activities of these organisms can profoundly affect Fe and As cycling in environmental systems, as they provide a sink for both Fe(II) and As (16). Reducing groundwaters with elevated levels of As also often exhibit elevated Fe(II) concentrations (17, 18) as a result of microbial Fe(III) reduction. Chemically, Fe(II) is a strong reductant and can readily undergo biotic or abiotic oxidation at circumneutral pH. Stimulating Fe(II) oxidation in these instances would result in the production of HFO and the subsequent removal of As through adsorption and coprecipitation. This concept has been demonstrated in experiments with lake sediments (16), as well as in sand-filled bioreactors inoculated with denitrifying sludge (11).

The ability of free sulfide to form insoluble metal sulfides has been applied in the remediation of industrial sites contaminated with metals such as zinc, cadmium, and nickel (19, 20). Typically, the remediation approach consists of supplying an electron donor and, in some cases, extra sulfate to stimulate microbial sulfate reduction. The resulting sulfide production then lowers the metal concentrations in solution through the formation of metal-bearing sulfide mineral phases. Sulfate reduction is carried out by a variety of organisms that are ubiquitous in marine and freshwater

Received 4 March 2013 Accepted 30 April 2013
Published ahead of print 10 May 2013
Address correspondence to Enoma O. Omoregie, omoregie@cab.inta-csic.es.
* Present address: Enoma O. Omoregie, Centro de Astrobiología, Madrid, Spain; Raoul-Marie Couture, Norwegian Institute for Water Research, Oslo, Norway.
Supplemental material for this article may be found at http://dx.doi.org/10.1128/AEM.00683-13.

doi:10.1128/AEM.00683-13

systems (21). In some naturally reducing aquifers, sulfate reduction is thought to control As levels through coprecipitation of As with sulfide minerals (22). Studies utilizing sediments (23), as well as field trials in Bangladesh (24), have shown that stimulating sulfate reduction can effectively decrease As concentrations *in situ* through the formation of As-bearing sulfide minerals.

Despite the potential effectiveness of biogenic HFO and sulfide minerals at sequestering As, there is little information on how these processes operate in natural aquifer systems. This information is important in order to develop viable remediation methods. The present study was undertaken to determine whether mineral formation induced by the addition of nitrate or a mixture of sulfate plus lactate could remediate As in a Southeast Asian aquifer system known to have elevated As levels in the groundwater (17, 25). We amended microcosms containing aquifer sediment with nitrate or sulfate plus lactate in order to generate *in situ* biogenic Fe(III) hydroxides/oxides and Fe(II) sulfide phases, respectively. We then examined changes in the resulting aqueous and solid-phase geochemistry, as well as microbial community structure, using an array of biogeochemical tools.

MATERIALS AND METHODS

Sediment collection. Sediment samples were collected in July 2008 from an aquifer system in Rotaing, Cambodia (GPS coordinates 105°03′6.70E, 11°27′17.62N), known to have elevated groundwater arsenic levels (17, 25). Previously reported As concentrations from this area were 0.2 to 18 μM (17, 25, 26). Samples were obtained down to 13-m depth by auguring. Once retrieved, the cores were flushed with N_2 gas, capped at both ends, and placed in vacuum-sealed plastic bags. Samples were stored at 4 to 10°C until the initiation of the microcosm studies.

Microcosm setup. Preliminary microcosm incubations were carried out to determine the potential release of soluble As from the sediments. Based on this preliminary screening, the sediments from the 12- to 13-m depth interval were selected for further study. The sediments were homogenized prior to their use in the microcosm experiments. Approximately 8 g of sediment was added to 20 ml of sterile artificial groundwater in 100-ml glass serum bottles. Microcosms were assembled in an anaerobic cabinet and, following the addition of sediment and synthetic groundwater, sealed with butyl rubber stoppers. The synthetic groundwater described by Islam et al. (8), which is similar to the natural groundwater composition in the area, was used for all microcosms. The headspace was then replaced with a 20:80 CO_2/N_2 mixture. All microcosms were incubated in the dark at 20°C for the duration of the experiment. The microcosms were initially run for a period of 28 days without any amendment. The purpose of this "mobilization phase" was to follow the natural release of As and other geogenic chemicals. Any microbial activity during this initial mobilization phase relied on endogenous substrates present naturally in the sediments.

Following the mobilization phase, the microcosms were run for an additional 115 days. For this "remediation phase," the microcosms were amended either with nitrate or with a mixture of sulfate plus lactate. The two treatments were intended to stimulate lithotrophic oxidation of Fe(II) present in the sediment in one case or heterotrophic sulfate reduction in the other. At the start of the remediation phase, the microcosms were amended in triplicate to approximately 10 mM sodium nitrate or approximately 10 mM sodium sulfate and 15 mM sodium lactate. On day 52 of the remediation phase, the nitrate-treated microcosms were further amended to approximately 11 mM sodium nitrate and the sulfate-plus-lactate microcosms to approximately 13 mM sodium sulfate and 15 mM sodium lactate. A triplicate set of microcosms was maintained without amendments as a control during the remediation phase. Note that the microcosms were thoroughly shaken prior to sampling. Samples for geochemical and microbial analysis were obtained by piercing the rubber stoppers with a needle and withdrawing 4 ml of the sediment slurry into a syringe. Details of microcosm treatment and analysis are given in Table S1 in the supplemental material.

Geochemical and mineralogical analyses. The pH and redox potential (Eh) of the slurries were measured on aliquots that were first removed from the microcosms in an anaerobic chamber and sealed in plastic tubes. The tubes were removed from the chamber, and then pH and Eh probes were inserted immediately after opening the tubes. The reported Eh values are expressed relative to the standard hydrogen electrode (SHE). Reactive ferrous iron was extracted with HCl using the ferrozine-based spectrophotometric method of Lovley and Phillips (27) by adding 39 μl of slurry to 1.9 ml of 0.5 M HCl. As defined by this study, HCl-Fe(II) is the Fe(II) released by the slurry in 0.5 M HCl after 90 min of reaction. For each microcosm, samples for cation and anion analyses were centrifuged to separate the supernatant from the sediment. Sulfide measurements (minimum detectable concentration limit, ~4 μM) were conducted on an aliquot of the supernatant using the Hach sulfide kit (Hach Lange, Germany). The supernatant was then filtered through a 0.45-μm-pore-size filter, and an aliquot was taken for As and cation (Fe, Mn, and Na), anion (sulfate, nitrate, lactate, propionate, and acetate), and ammonium analyses. Samples for As and cation analysis were acidified to pH ~2 with 0.5 M nitric acid and stored at 4°C until analysis. Acidification of aqueous samples containing As and sulfide can lead to the precipitation of arsenic sulfides (28) and hence to an underestimation of the total dissolved As concentration. However, this effect is assumed to be small, as the experimental solutions were characterized by measurable dissolved Fe concentrations while aqueous sulfide concentrations were always below the detection limit. Cation and As concentrations were determined by inductively coupled plasma mass spectrometry (ICP-MS) on an Agilent (United Kingdom) 7500cx instrument. Anion analysis was carried out by ion chromatography on a Dionex 600 instrument (Dionex, United Kingdom). Ammonium was measured using Nessler's reagent (Hach Lange). Methane concentrations were measured by injecting 100 μl of the headspace gas into an Agilent (United Kingdom) 5890A gas chromatograph coupled to a 5975C mass spectrometer.

Residual sediment from sequential extractions was frozen at −80°C for analysis by X-ray absorption near edge structure (XANES) and extended X-ray absorption fine structure (EXAFS) spectroscopy, X-ray photoelectron spectroscopy (XPS), X-ray diffraction (XRD), and Mössbauer spectroscopy. The bulk composition of the solid starting materials was also determined on air-dried, finely ground pressed-powder briquettes by X-ray fluorescence spectrometry. Details of analyses using these methods are given in File S1 in the supplemental material.

Microbial community analysis. After centrifugation, a portion of the sediment remaining in each microcosm was frozen at −80°C until microbiological analysis could be carried out. Total DNA was extracted from approximately 250-mg sediment subsamples using the PowerSoil DNA kit (Mobio, Carlsbad, CA). The extractions were performed according to the manufacturer's recommendations. Bacterial 16S rRNA genes were amplified from total extracted DNA using the GM3 (AGAGTTTGATCMTGGC) and GM4 (TACCTTGTTACGACTT) primers. PCR cloning and sequencing were carried out following the protocol of Niemann et al. (29). Phylogenetic analysis was carried out using the ARB (30) software package with the Silva 98 release database (31).

Geochemical modeling. Calculations at equilibrium and transport-reaction modeling were performed using the public domain computer code PHREEQC version 2.17.5. Eh-pH diagrams were generated using the beta version of the public domain computer code PhreePlot. The thermodynamic database WATEQ4F embedded within PHREEQC was updated by including equilibrium constants for the ionization of As(III) and As(V) oxyacids (32), the sulfidation of As species, Fe mineral solubilities, and As mineral solubilities. A compilation of the relevant equilibrium constants is given by Couture et al. (33). To our knowledge, there is no definitive ensemble of thermodynamic constants to predict As speciation in sulfidic waters. We chose to include the thermodynamic data set provided by Helz and Tossell (34), which predicts the coexistence of As(V) and As(III)

TABLE 1 Summary of 16S rRNA gene sequences obtained from selected samples

Phylogenetic affiliation and representative isolate(s)[a]	GenBank accession no.	% identity[b]	No. of sequences obtained			
			Mobilization phase	Untreated sample	Nitrate-treated sample	Sulfate- and lactate-treated sample
Beta- and *Gammaproteobacteria*						
Azospira oryzae	AY277622	95–99	7	32	20	22
Sideroxydans lithotrophicus	DQ386859	95–99	0	4	17	0
Other			2	2	4	0
Epsilonproteobacteria						
Sulfurospirilllum NP4	AY756183	95–99	1	0	1	0
Deltaproteobacteria						
Geobacter sulfurreducens	U13928	95–99	8	2	2	1
Geobacter uraniireducens Rf4	CP000698	95–99	10	1	1	1
Desulfobulbus propionicus			0	0	0	0
Desulfovibrio putealis	AY574979	95–99	0	0	0	12
Bacteroidetes			3	0	1	0
Clostridiales			14	4	0	10
Total			45	45	46	46

[a] Sequence chosen from an isolate that is closely related to the sequences obtained in this study.
[b] Approximate identity between the sequences from the microcosms and the representative isolate.

thioanions, even though more experimental support is needed to confirm the accuracy of the prediction. Because of the inherent uncertainties of this thermodynamic database, we refer to the predicted species collectively as thioarsenicals.

A diffuse double-layer surface complexation model (DDLM) comprising consistent sets of intrinsic adsorption constants was developed to predict As partitioning between the dissolved phase and the biogenic iron solids. In this calculation, performed with the code PHREEQC, we used our geochemical measurements for the microcosms as input parameters, along with intrinsic constants for adsorption of As(III) and As(V) species onto HFO (10). The model parameters for HFO assumed a specific surface area of 600 $m^2\ g^{-1}$ for HFO, a strong-site density of 0.005 mol mol Fe^{-1}, and a weak-site density of 0.2 mol mol Fe^{-1}.

A one-dimensional transport-reaction model was built in PHREEQC to scale the As removal rates observed in our microcosms up to an aquifer flow line. The physical parameters imposed in the calculations are those of the sandy Cambodian aquifer described by Polizzotto et al. (25). The reaction network included the reactions described above, as well as (i) the rate of microbially mediated oxidation of Fe(II) by nitrate and that of sulfate reduction measured in the microcosms and (ii) equilibrium isotherms (K_d [partition coefficient] and surface complexation based) describing the partitioning of As between the dissolved and particulate phases (see Table S2 in the supplemental material).

Nucleotide sequence accession numbers. The sequences generated in this study have been deposited in the GenBank database and are accessible under accession numbers JQ976293 to JQ976474.

RESULTS

Solid-phase characterization of starting materials. The aquifer sediments used in this study were characterized in detail prior to starting the incubation experiments. The sediments were dark-brown, finely grained sands. Powder XRD (see Fig. S1 in the supplemental material for an example of a diffractogram) identified crystalline phases similar to those reported for aquifer sediments from Cambodia (35). The sediment mineralogy was dominated by quartz (SiO_2), with lesser amounts of alkali feldspar [$(K,Na)AlSi_3O_8$], muscovite [$KAl_2(Si_3Al)O_{10}(OH,F)_2$], and clinochlore [$(Mg,Fe)_5Al(Si_3Al)O_{10}(OH)_8$] or related chlorite-type minerals. The XRD data were consistent with bulk chemical analyses with XRF (details not shown) that indicate major amounts of silicon and aluminum and smaller amounts of K, Na, Mg, and Ca. The sediment also contains a relatively high total Fe concentration of ~5.5 wt%. Also of particular relevance are the relatively high concentrations of Mn (~ 850 ppm) and As (~15 ppm).

Biogeochemical changes during the mobilization phase. All microcosms were incubated without amendment for 28 days in order to mobilize arsenic and other metals/metalloids. During this initial phase, concentrations of soluble As, Fe, and Mn increased by 70 to 270%, to 1.91 ± 0.5, 768 ± 59, and 18.4 ± 2.23 μM, respectively (see Fig. S2 in the supplemental material). Redox conditions within the microcosms became more reducing, with Eh decreasing from approximately +109 to approximately +52 mV (with respect to the standard hydrogen electrode). The microbial community composition determined from a sample taken at the end of the mobilization phase (Table 1) revealed the presence of anaerobic organisms capable of As(V), Mn(IV), and Fe(III) reduction, including *Geobacter* (36, 37) and *Sulfurospirillum* (38, 39) species. In addition, sequences related to fermentative bacteria, such as *Clostridiales*, were also significant components of the 16S rRNA gene sequence library at the end of the mobilization phase.

Aqueous geochemistry during the remediation phase. After the initial 28-day mobilization phase, the microcosms were monitored for an additional 115 days, with and without treatment. Without treatment, soluble As, Fe, and Mn concentrations continued to increase, ultimately reaching 3.9 ± 0.9, 910 ± 33, and 22 ± 3 μM, respectively (Fig. 1A). The pH remained relatively stable during this period at ~6.6. These concentrations and the pH values are comparable to measurements reported for groundwater from the area where the microcosm sediment was collected (25).

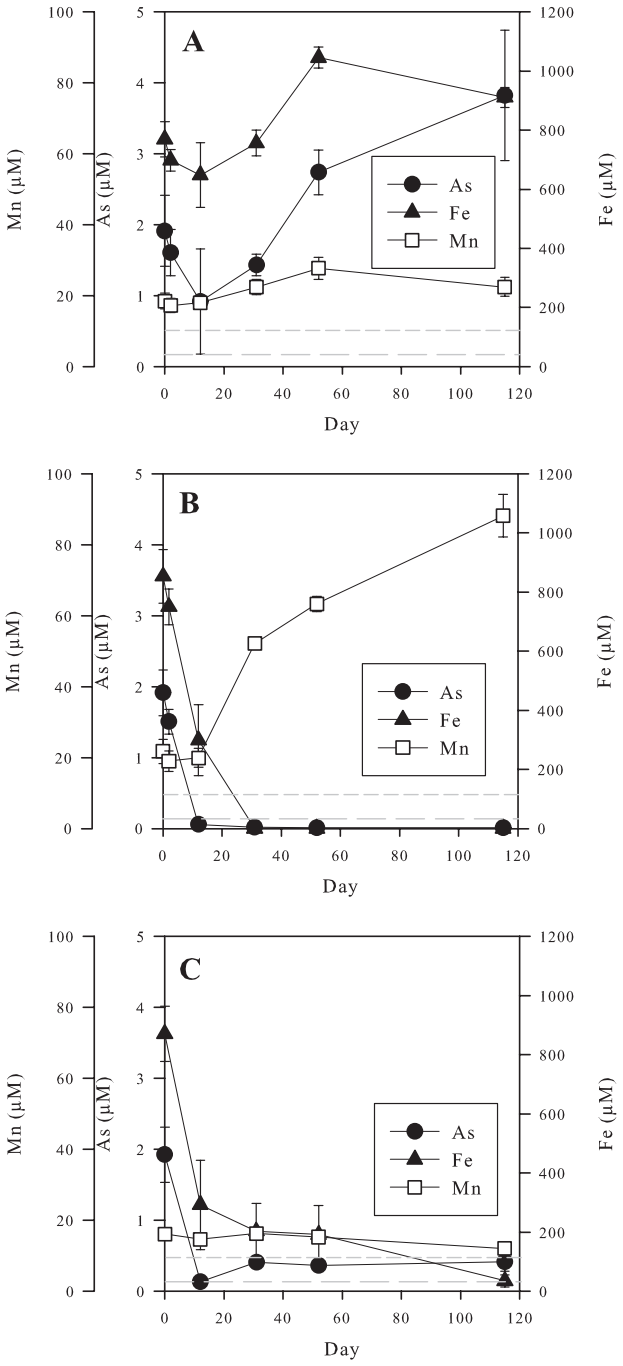

FIG 1 Soluble arsenic, iron, and manganese concentrations for the untreated (A), nitrate-treated (B), and sulfate-plus-lactate-treated (C) microcosms. The origin of time on the graphs corresponds to the start of the remediation phase. Average results from three separate microcosms are plotted. The error bars are standard deviations of the results from the three microcosms. The long dashed horizontal lines indicate the WHO guideline maximum acceptable concentration for As, and the short dashed lines indicate the WHO guideline maximum concentration for Mn.

In contrast to the unamended microcosms, those supplied with nitrate turned from dark to light brown within 12 days, consistent with the formation of ferric iron hydroxides/oxides. At the same time, soluble As and Fe concentrations (Fig. 1B) in these microcosms dropped to 0.06 ± 0.02 and 298 ± 120 μM, respectively. The soluble As and Fe concentrations decreased further until day 32 and remained relatively constant throughout the rest of the remediation phase, despite the presence of about 9 mM nitrate. Soluble Mn concentrations in the nitrate-treated microcosms increased substantially, reaching 63 ± 2 μM by the end of the remediation phase.

The microcosms in which sulfate reduction was stimulated turned black within 12 days, suggesting the precipitation of iron sulfide (most likely FeS, or mackinawite) as a result of the biogenic production of sulfide. Soluble As and Fe concentrations in the sulfate-reducing systems fell to 0.13 ± 0.07 and 292 ± 150 μM, respectively, 12 days after the first addition of sulfate and lactate (Fig. 1C). However, arsenic concentrations increased to 0.41 ± 0.02 μM by day 31 and remained at this level even when additional sulfate and lactate were added. Soluble Fe concentrations continued to decrease, reaching 34 ± 20 μM by day 115. Soluble Mn concentrations in the sulfate-reducing microcosms decreased slightly.

Nitrate concentrations in the nitrate-treated "oxidative" microcosms fell to about 2 mM by day 52 of the remediation phase (Fig. 2A). On day 52, the microcosms were again supplemented with nitrate; however, no significant further nitrate removal was observed between day 52 and the end of the experiment (day 115). No significant nitrate consumption was observed in nitrate-amended but autoclaved microcosms (see Fig. S3 in the supplemental material). In the sulfate-plus-lactate-amended microcosms, lactate was exhausted by day 12 of the remediation phase (Fig. 2B). Concentrations of acetate and propionate (Fig. 2C), which are breakdown products of lactate metabolism, increased during this period. By day 52, acetate, lactate, and sulfate concentrations had all dropped substantially. Following the second addition of sulfate and lactate, sulfate concentrations dropped from 13 mM to about 5 mM, implying that a further 8 mM sulfate had been consumed by day 115. Lactate, propionate, and acetate were below the detection limit at this point. Methane gas [$CH_{4(g)}$] concentrations determined from headspace measurements on day 115 were 3.3 mmol liter^{-1} in the sulfate and lactate microcosms, in contrast to less than 0.3 mmol liter^{-1} in all other microcosms. No significant sulfate consumption was observed throughout the experiment in sulfate- and lactate-amended but autoclaved microcosms (see Fig. S3 in the supplemental material). However, significant lactate consumption was observed between days 52 and 120 in these autoclaved microcosms.

Acid-extractable ferrous iron [HCl-Fe(II)] in the untreated microcosms fluctuated between 43 and 53 mmol kg slurry^{-1} during the course of the remediation phase (Fig. 3). In the nitrate-treated microcosms, HCl-Fe(II) concentrations decreased from 43 to about 16 mmol kg slurry^{-1} by day 52. However, by day 115, they had increased again slightly to about 25 mmol kg slurry^{-1}, which was still significantly below the starting concentration. HCl-Fe(II) concentrations in the sulfate- and lactate-treated microcosms decreased to about 30 mmol kg slurry^{-1} by day 115.

The redox potentials, Eh, in the untreated and the sulfate-plus-lactate-treated microcosms fell to approximately 27 and 8 mV, respectively, by the end of the remediation phase. In contrast, the Eh rose to around 216 mV during this period in the nitrate-treated microcosms. The pH in the untreated and nitrate-treated microcosms was relatively stable at 6.6 during the remediation phase. However, the pH increased from about 6.6 to 7.3 in the sulfate-plus-lactate-treated microcosms.

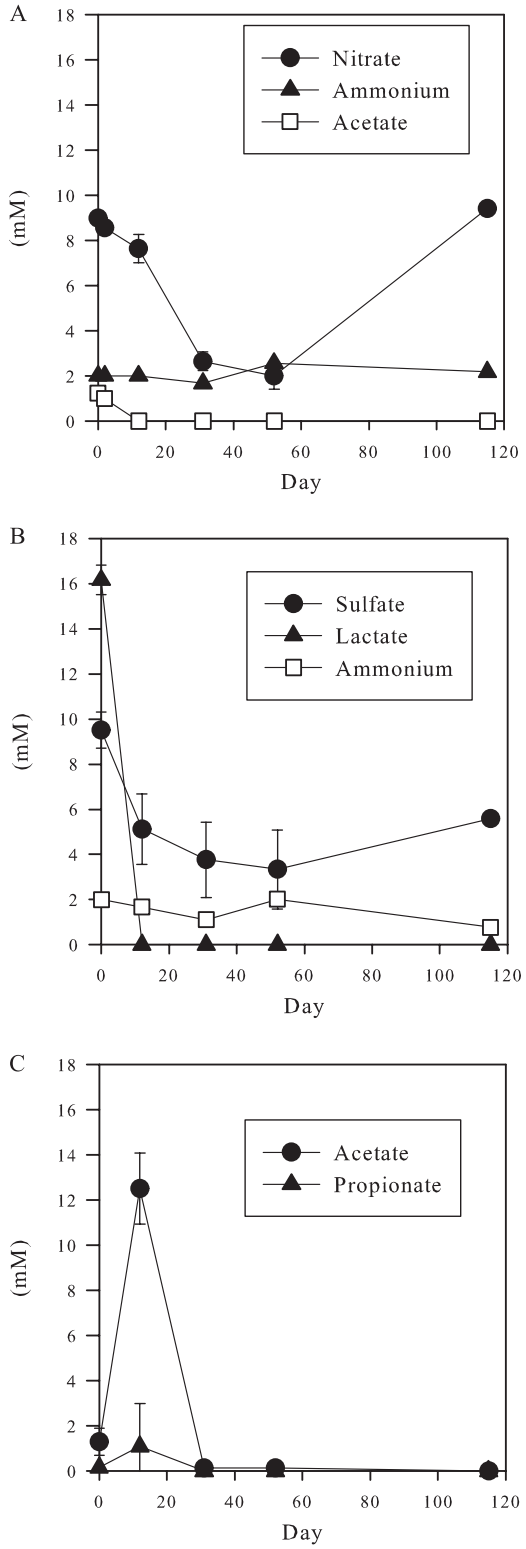

FIG 2 Anion and ammonium measurements from the nitrate-treated (A) and sulfate-plus-lactate-treated (B and C) microcosms. The origin of time on the graphs corresponds to the start of the remediation phase. Average results from three separate microcosms are plotted. The error bars are standard deviations of the results from the three microcosms. On day 52 of the remediation phase, the microcosms were further amended to approximately 11 mM sodium nitrate, or approximately 13 mM sodium sulfate and 15 mM sodium lactate, respectively.

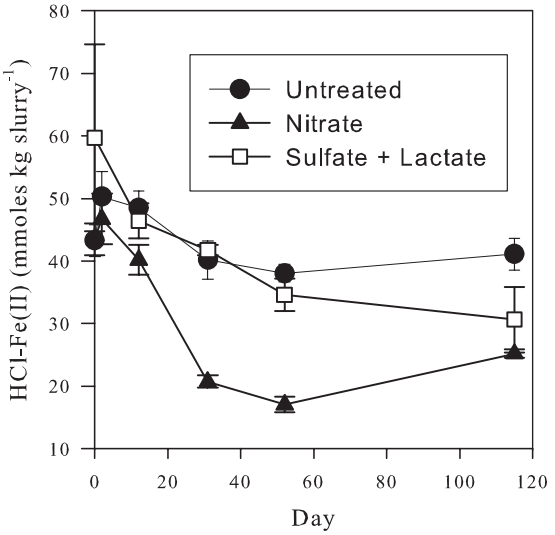

FIG 3 HCl-extractible Fe(II). The plots are of the untreated, nitrate-treated, and sulfate-plus-lactate-treated microcosms. The origin of time on the graphs corresponds to the start of the remediation phase. Average results from three separate microcosms are plotted. The error bars are standard deviations of the results from the three microcosms.

Characterization of remediation-phase solids. No significant changes were observed in the XRD spectra obtained following the different remediation treatments. This is not surprising, considering that the sediment mineralogy is dominated by detrital (quartz, feldspar, muscovite mica, and clay mineral) phases that are largely nonreactive on the time scale of the incubation experiments. It further suggests that any secondary phases formed during the experiments were amorphous or poorly crystalline and probably produced in very small amounts.

The spectroscopic techniques used to characterize the solid phases are powerful probes of the two main elements of interest, iron and arsenic. All the Mössbauer spectra (see Fig. S4 in the supplemental material) were fitted first with a sextet of peaks indicative of a magnetically ordered iron mineral. The hyperfine field value (516 kilooersteds [kOe]) suggests that this phase is hematite, while the peak intensities (areas) show that it represents ~20% of the total Fe (hence, ~1% of the solid material). The magnetically ordered iron phase remained unchanged in character and relative concentration after all treatments, suggesting that it was not available for bioreduction. The other peaks were best fitted with doublets, two with larger isomer shifts (~1.02 to 1.25 mm s^{-1}) and quadrupole splittings (~1.9 to 2.5 mm s^{-1}), indicative of Fe^{2+} in a silicate (chlorite) phase, and one with a much smaller isomer shift (0.34 to 0.41 mm s^{-1}) and quadruple splitting (0.37 to 0.54 mm s^{-1}), indicative of Fe^{3+}. The main differences in Mössbauer spectra between the endpoints of the nitrate and sulfate-plus-lactate treatments were in the relative intensities of the peaks attributable to Fe^{2+} and Fe^{3+}. The key observation was that the Mössbauer spectra of the nitrate-treated microcosms implied a markedly higher abundance of Fe^{3+} (49%) than in those of the sulfate-plus-lactate-treated microcosms (39%). The latter also showed increased Fe^{2+} (42%) compared to the nitrate-treated microcosms (32%). For comparison, the Mössbauer spectrum of a sample from the untreated microcosms yielded intermediate abundances of Fe^{3+} (43%) and Fe^{2+} (37%).

TABLE 2 Arsenic K-edge EXAFS fit[a]

Sample	Fit	Scatterer	*n*	*r* (Å)	$2\sigma^2$ (Å^2)	*R* factor
Reference sediment[b]		O	4	1.70	0.014	37.1
Untreated		O	3	1.74	0.010	46.8
Nitrate	1-shell	O	4	1.70	0.010	35.1
	2-shell	O	4	1.70	0.010	30.4
		Fe	2	2.96	0.052	
Nitrate[c]		O	4	1.71	0.002	47
Sulfate plus lactate	1-shell	O	3	1.68	0.017	52.7
	2-shell	O	2.4	1.69	0.010	39.5
		S	0.8	2.25	0.003	
Sulfate plus lactate[d]	1-shell	O	3	1.72	0.019	70.7
	2-shell	O	2	1.73	0.009	47.5
		S	1.3	2.28	0.009	

[a] All samples were taken from the microcosms on day 115. Error for number of scatterers (*n*), ±25%; error for arsenic scatter distance (*r*), ±0.02 Å for first shell, ±0.05 Å for outer shell; error for Debye-Waller-type factor ($\Sigma 2\sigma^2$), ±25%. *R* factor, residual (indicator of goodness of fit).
[b] Sediment frozen at the start of the experiment and used as a reference for manipulated sediment.
[c] Sequentially extracted to remove nonspecifically sorbed As, exchangeable specifically sorbed As, and As bound to amorphous and poorly crystalline hydrous oxides of Fe and Al.
[d] Sequentially extracted to remove nonspecifically sorbed As, exchangeable specifically sorbed As, As bound to amorphous and poorly crystalline hydrous oxides of Fe and Al, and As bound to well-crystallized hydrous oxides of Fe and Al.

TABLE 3 Mössbauer fitting and XANES fitting of As K-edge XAS data[a]

Sample	Mossbauer fitting [% Fe(II)]	XANES fitting (% arsenic in form of:)			
		Arsenate	Arsenite	As-S	FeAsS
Reference sediment[b]	NA[e]	53	47	–[f]	–
Untreated	37	16	84	–	–
Nitrate	32	64	36	–	–
Nitrate[c]	NA	28	72	–	–
Sulfate plus lactate	42	16	65	19	–
Sulfate plus lactate[d]	NA	10	54	36	–

[a] All samples were taken from the microcosms on day 115. The fit index is $S\,[(I_{obs} - I_{calc})2]/n$, where *n* is the number of points in each spectrum. Errors for proportions of standards are ca. ± 10.
[b] Sediment frozen at the start of the experiment and used as a reference for manipulated sediment.
[c] Sequentially extracted to remove nonspecifically sorbed As, exchangeable specifically sorbed As, and As bound to amorphous and poorly crystalline hydrous oxides of Fe and Al.
[d] Sequentially extracted to remove nonspecifically sorbed As, exchangeable specifically sorbed As, As bound to amorphous and poorly crystalline hydrous oxides of Fe and Al, and As bound to well-crystallized hydrous oxides of Fe and Al.
[e] NA, data not collected.
[f] –, not detected.

The XPS data (Fe^{2+} peaks) for the same samples as studied using Mössbauer spectroscopy confirmed the above observations regarding the relative abundances of the oxidation states of iron (see Fig. S5 in the supplemental material). According to the XPS data, the Fe^{3+} percent contribution determined at the end of the nitrate treatment was 54%, compared to 49% for the sulfate-plus-lactate treatment (and 51.5% for untreated microcosms).

Solid-phase As speciation was determined using X-ray absorption at the arsenic K edge (Table 2; see Fig. S6 and S7 in the supplemental material). From the fitting of XANES spectra (Table 3; see Fig. S8 in the supplemental material), arsenic speciation was apportioned between arsenite [(As(III)], arsenate [As(V)], and arsenic bonded to sulfur. The arsenite/arsenate ratios for untreated and nitrate-treated microcosms were 84:16 and 36:64, respectively. For the sulfate-plus-lactate-treated microcosms, the fitting implied that 19% of As was bound to sulfide, 65% was arsenite, and 16% was arsenate. These values agree with the geochemical and redox changes expected for the various treatments. Although some of the *R* values reflect the high level of noise in the spectra (due to the low concentration of As), meaningful information on the local bonding environment of As in the samples was derived from fitting of the EXAFS spectra (see Fig. S6 in the supplemental material). In all cases, the first shell of atoms surrounding the arsenic consisted of oxygen at distances of 1.70 to 1.74 Å. The untreated microcosm yielded a fit with just a single shell of 3 oxygen atoms at 1.74 Å. However, for the remediation treatments, a better fit was achieved with two shells of atoms. In the case of the sulfate-plus-lactate treatment, this involved sulfur atoms at 2.25 Å, supporting the XANES evidence for arsenic closely associated with a newly formed sulfide phase.

Speciation of As at the end of the sulfate-plus-lactate treatment was also analyzed using sequential chemical extractions (see File S1 in the supplemental material) coupled with XANES and EXAFS analyses. The chosen extraction protocol successively removes nonspecifically sorbed As, specifically sorbed As, As bound to amorphous and poorly crystalline hydrous oxides of Fe and Al, and As bound to well-crystallized hydrous oxides of Fe and Al. The extraction protocol does not remove As bound to sulfides and organics. Note that XANES and EXAFS analyses were performed on the residual solid materials from the sequential extractions. The XANES analysis showed a decrease in the proportions of arsenite and arsenate and an increase in the proportion of sulfur-bound arsenic compared to the nonsequentially extracted sulfate-plus-lactate treatments. These results suggest that the arsenate and arsenite that were not removed by the sequential extraction were likely associated with a sulfide phase, possibly FeS.

In the case of the nitrate treatment, the second shell consisted of Fe atoms at 2.96 Å, as reported previously for As(V) inner-sphere complexation to goethite surfaces (40). The EXAFS analysis also yielded a first-shell As-O distance of 1.70 Å, confirming a greater proportion of As(V). A sample from the nitrate-treated microcosms was also analyzed after performing the same sequential extraction described above for the sulfate-plus-lactate treatment, but without the step to remove As bound to well-crystallized hydrous oxides of Fe and Al. As a result of the extraction, the ratio of arsenate to arsenite decreased to 28:72, showing a loss of arsenate, which suggests that arsenate in the nitrate treatments was mainly bound to the freshly formed HFO. EXAFS showed a single shell of oxygen scatterers at 1.71 Å; the slightly longer bond length was also consistent with an increased proportion of arsenite.

Microbial community structure during the remediation phase. 16S rRNA gene sequence analyses of samples from all microcosms were dominated (15 to 71%) by sequences from organisms closely related to *Azospira oryzae* (Table 1). Furthermore, organisms closely related to metal [Fe(III) and As(V)]-reducing bacteria, such as *Geobacter* sp. (36, 37) and *Sulfurospirillum* sp. (38, 39), were present in all microcosms. Sequences closely related to those of Fe(II)-oxidizing bacteria, such as *Sideroxydans* (41, 42), were detected in the untreated and nitrate-treated microcosms only. However, the percentage of these organisms in the nitrate-

treated microcosms was much higher than in the untreated microcosms (37% as opposed to 9%). Organisms closely related to the sulfate-reducing bacterium *Desulfovibrio putealis* (21) were detected only in the sulfate-plus-lactate-treated microcosms. Sequences closely related to fermentative bacteria, such as *Clostridiales*, were also significant components (9 to 22%) of the 16S rRNA gene sequence library for both the untreated and the sulfate-plus-lactated-treated microcosms.

Thermodynamic modeling. Based on the experimental results, reaction pathway models were used to gain insight into As and Fe speciation during the experiments. We calculated the saturation indices (SI) (SI = log IAP/K_{sp}, where IAP is the ion activity product and K_{sp} the solubility product) of the aqueous phase with respect to various mineral phases. This modeling exercise revealed that the nitrate-treated microcosms became supersaturated with respect to various Fe(III)-oxyhydroxides (HFO, two-line ferrihydrite, lepidocrocite, hematite, and goethite) during the course of the nitrate-amended experiments. Assuming As sorption onto freshly precipitated HFO, the equilibrium As partitioning between the dissolved and solid phases using surface complexation modeling yielded a dissolved As concentration of 24 nM and an amount of adsorbed As of 1.9 μmol (per liter slurry), respectively. Figure 4A shows the measured Eh and pH values superimposed on a theoretical Eh-pH diagram for As and Fe for the nitrate-amended microcosms. For the initial system conditions, geochemical modeling predicts that the dissolved species $H_2AsO_4^{-}{}_{(aq)}$ dominated As speciation. With the progression of the experiment, the Eh-pH trend crossed the $Fe^{2+}/Fe(OH)_{3(s)}$ boundary, moving toward the stability fields of $Fe(OH)_{3(s)}$. At the end of the experiment, the speciation calculations implied that As speciation was dominated by As bound to HFO surfaces ($FeO{\equiv}OHAsO_4^{3-}$).

Because aqueous sulfide remained below the detection limit of 4 μM over the course of the sulfate-plus-lactate treatment, we assumed in the thermodynamic-speciation model that all sulfide generated from sulfate reduction reacted with Fe, present in excess, to form disordered mackinawite [$FeS_{m(s)}$]. This is a reasonable assumption, as $FeS_{m(s)}$ is widely considered to be the first Fe sulfide to form in most low-temperature geochemical environments. The amount of $FeS_{m(s)}$ calculated from the sulfate consumption was 14 mmol (~1,200 ppm). Based on this estimate, and on a log K_{sp} of 3.5 for $FeS_{m(s)}$ (43), we then calculated an equilibrium sulfide analysis in the presence of excess Fe^{2+} concentrations of 34 μM at pH 7.2. It is useful to estimate the free sulfide concentration, as sulfide can form complexes with dissolved As(V) and hence potentially increase As solubility (44). The calculation of the SI with respect to arsenic sulfide minerals (orpiment, realgar, and arsenopyrite) revealed that these phases were undersaturated by several orders of magnitude (SI ≤ 6) and hence were unlikely to form. In the absence of As-sulfide minerals, As adsorption onto the surface of $FeS_{m(s)}$ represents a likely mechanism explaining the drop in dissolved As (33, 45, 46). Based on the linear isotherm for As adsorption onto $FeS_{m(s)}$ of Wolthers et al. (45), we then predicted an equilibrium aqueous As concentration range of 0.7 to 3.0 μM (isotherm, K_d = [As]/[As-$FeS_{m(s)}$], where [As-$FeS_{m(s)}$] is the concentration of adsorbed As).

As described above for the nitrate system, a reaction pathway model for the sulfate-plus-lactate-amended microcosm experiments was constructed using the experimental results as constraints (Fig. 4B). In the absence of As sulfide mineral precipitation, the Eh-pH plots indicate that $H_3AsO_3^0$ and SO_4-green rust should dominate As and Fe speciation, respectively, throughout

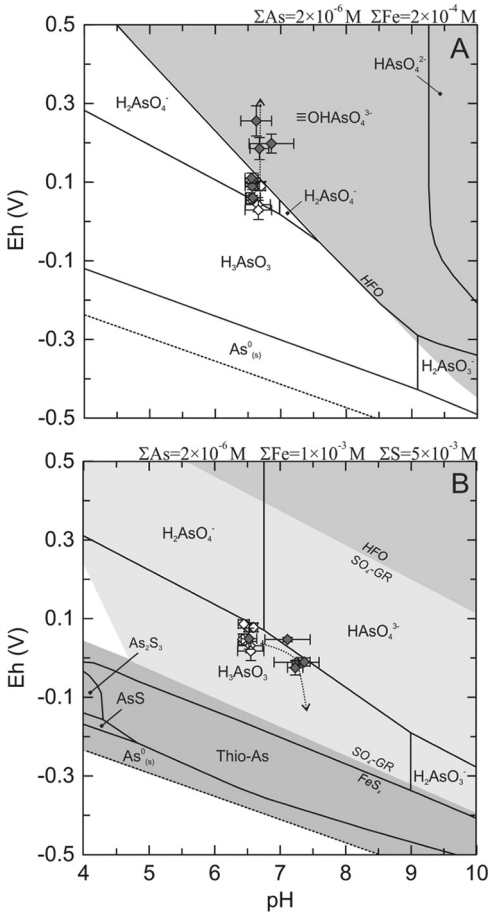

FIG 4 Reaction pathway models at 25°C for the nitrate-treated (A) and sulfate-plus-lactate-treated (B) microcosms. The filled diamonds are calculated Eh and pH values for the nitrate- and sulfate-plus-lactate-treated microcosms. The open diamonds are Eh-pH couples for the untreated microcosms. Each point is the average of the three replicate microcosms, and the error bars are the standard deviations of those measurements. The dotted lines with arrows indicate the pathways of the reactions. The solid lines delineate the stability fields of various As and Fe species. The symbol ≡ indicates a sorption complex. FeS_x represents the combined stability fields of $FeS_{m(s)}$ (mackinawite) and FeS_2 (pyrite).

the experiment. Note that, although pyrite (FeS_2) is thermodynamically more stable than $FeS_{m(s)}$, the latter is the first to form and therefore tends to control the solution chemistry. To reflect this, the stability fields of $FeS_{m(s)}$ and FeS_2 (pyrite) have been merged in Fig. 4B.

Transport-reaction modeling. The rate of nitrate consumption in the nitrate-amended microcosms was on the order of 0.14 mmol NO_3 day^{-1}. This rate of nitrate consumption was implemented in a one-dimensional transport-reaction model to simulate chemical changes along a flow line in the aquifer, assuming that all nitrate reduction is coupled to the oxidation of bioavailable Fe(II). This is reasonable, given that the observed ratio of nitrate consumption (Fig. 2A) to HCl-Fe(II) (Fig. 3A) consumption is about 1:4.3 in the first 52 days of the remediation phase. This is similar to the 1:5 ratio for microbial nitrate reduction coupled to Fe(II) oxidation reported previously (13, 14). The reaction was allowed to proceed until depletion of all the available solid-phase Fe(II) (Fig. 5A). The aqueous Fe(III) produced then precip-

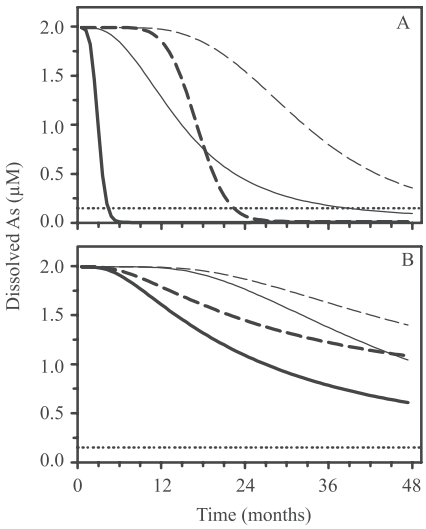

FIG 5 Model predicted As concentration as a function of time along an aquifer flow line at 50 m (solid lines) and 100 m (dashed lines) from the site of a continuous nitrate (A) or sulfate-plus-lactate (B) injection. The concentrations of sulfate and nitrate injected are either fixed at those used in the microcosms (thick lines) or at the recommended WHO level for drinking water (thin lines). The horizontal dotted lines indicate the recommended WHO provisional guide value for As in drinking water (0.13 μM).

itates as $Fe(OH)_{3(s)}$, which sorbs dissolved As according to the surface complexation model described above. Similarly, the rate of microbially mediated SO_4^{2-} reduction (~0.12 mmol SO_4^{2-} day^{-1}) was estimated from the initial drop in sulfate concentration with time. The reaction was implemented into the transport-reaction model (Fig. 5B), further assuming that all aqueous sulfide produced reacts with available Fe(II) to form $FeS_{m(s)}$. Removal of As from solution was assumed to follow the linear isotherm reported by Wolthers et al. (45).

DISCUSSION

The microbial communities inhabiting the Cambodian aquifer sediments studied in this work respond to the supply of nitrate by producing Fe(III)-oxyhydroxides/oxides and to the supply of sulfate plus lactate by producing sulfide, which in turn causes the precipitation of iron sulfide mineral phases. The formation of these mineral products clearly has a significant impact on soluble As concentrations; however, the observed geochemical and microbiological changes, and the implications for *in situ* As remediation, differ substantially between the two treatments.

Arsenic mobilization. Soluble As concentrations increased in all microcosms during the pretreatment phase (i.e., prior to the amendments). In the untreated microcosms, the As concentration continued to rise over the next 115 days of the experiments to a final value of 3.9 ± 0.9 μM. This soluble As concentration is well above the WHO provisional guideline safe value of 10 ppb (0.13 μM). It is comparable to groundwater arsenic concentrations that have been reported from this area of Cambodia (0.2 to 18 μM) (17, 25, 26). Microbially mediated reductive processes apparently cause the release of soluble As, together with that of soluble Fe and Mn (Fig. 1A). This is supported by three independent lines of evidence: (i) the presence of close relatives of bacteria known to carry out microbial As(V), Fe(III), and Mn(IV) reduction, such as *Geobacter uraniireducens* (36, 37), *Geobacter sulfurreducens* (36), and *Sulfurospirillum* sp. strain NP4 (38) (Table 1); (ii) the measured increases in solid-phase Fe(II) and As(III); and (iii) the drop in redox potential. Taken together, the available observations suggest that metal-reducing bacteria were responsible for the reductive transformations of As-, Fe-, and Mn-bearing minerals, in line with previous work that has implicated these organisms in As and Fe release in reduced sediments from Southeast Asian aquifers (8, 47).

The electron donors involved in the redox processes driving As mobilization are currently not well defined. Given the presence in the nonamended microcosms of up to 1 mM acetate (data not shown) and fermentative bacteria, such as members of the *Clostridiales*, it is likely that the electron donors for this process include organic compounds. Previous work has shown that a wide range of organic compounds likely play a role in microbial metal reduction (8, 35, 48). The increase in the relative number of sequences related to that of *A. oryzae* suggests the involvement of these organisms. These sequences were detected in all the microcosm samples that were examined. *A. oryzae* species are known heterotrophic nitrogen-fixing bacteria; however, the exact role they play in our microcosms cannot be derived from our experimental results.

Arsenic removal: HFO. Ferric iron hydroxides/oxides have been shown to be highly effective in lowering As levels in groundwaters (11, 12). This is consistent with the results from the nitrate-amended microcosms. In sharp contrast to the untreated microcosms, the addition of nitrate caused the removal of soluble As and Fe (Fig. 1B). Within12 days after the addition of nitrate, As and Fe concentrations in the aqueous phase dropped by 97 and 65%, respectively. By day 52, aqueous As concentrations were on the order of 0.01 μM, that is, well below the WHO guideline. The simultaneous removal of aqueous As and Fe can be attributed to microbial nitrate-dependent Fe(II) oxidation and the subsequent formation of HFO or a related ferric iron mineral phase. The measured decreases in nitrate (Fig. 2A) and HCl-Fe(II) (Fig. 3) of about 7 and 30 mM, respectively, within the first 52 days after nitrate amendment yield a ratio of 1:4.3. Given the uncertainties associated with the HCl-Fe(II) measurements, this ratio is consistent with the 1:5 ratio for microbial nitrate reduction coupled with Fe(II) oxidation reported previously (13, 14). Furthermore, nitrate amendment caused a significant increase in the percentage of sequences related to those of the Fe(II)-oxidizing bacterium *Sideroxydans lithotrophicus* LD-1 (41, 42) compared to the untreated microcosms (37% as opposed to 9%). Bacteria related to *S. lithotrophicus* have been implicated in Fe(II) oxidation in nitrate enrichment cultures (49). Taken together, these observations suggest that these organisms played a direct role in nitrate-dependent Fe(II) oxidation in the studied microcosms.

The equilibrium speciation modeling (Fig. 4A) further supports the conclusion that the addition of nitrate resulted in more oxidizing conditions, hence promoting microbial iron oxidation and subsequent sequestration of As(III) by HFO. The oxidation of As(III) and Fe(II) is also supported by the XANES and Mössbauer spectra, respectively, which show higher As(V) and Fe(III) concentrations than the untreated microcosms. Finally, XANES spectra obtained on the residual solids collected after the sequential extraction that removes nonsorbed As, exchangeable sorbed As, and As bound to HFO showed that the ratio of arsenate to arsenite dropped significantly (Table 3). Although the extractions were not performed quantitatively, these results suggest that the majority of

arsenic removed during the chemical extraction was in the form of arsenate bound to HFO.

The increase in Fe(III) could involve iron in clay minerals, in addition to the formation of HFO. Mössbauer spectroscopy cannot be used to discriminate between these two possibilities, because the amount of Fe that changed oxidation state during the nitrate treatment is too small, only on the order of 1,100 ppm, or ~2% of the total Fe. The evidence for HFO formation, although strong, is thus indirect. For example, the calculated saturation indices indicate that the aqueous phase became supersaturated with respect to HFO over the course of the nitrate treatment. Furthermore, surfaces of fresh HFO have a strong affinity for As (10).

Arsenic sorption onto HFO is also consistent with EXAFS spectra, which indicate that a portion of As is bound to an Fe phase. Although the bond length of 2.96 Å is different from that reported (3.25 Å) by Waychunas et al. (50), the latter study was conducted at significantly higher concentrations of As. Different As binding mechanisms, for example, face-sharing polyhedra (three oxygen bridges and shorter arsenic-iron distance) versus corner-sharing polyhedra (one oxygen bridge) could explain the discrepancy in As-Fe distance. The As-O bond length shows only an insignificant increase, from 1.70 to 1.71 Å, after the sequential extraction (Table 2): the length implies that there is still a mixture of As(V) and As(III) oxide species present, and the increase, though small, is consistent with an increased proportion of As(III), as shown by the XANES fitting. The binding of arsenic onto an Fe phase is also consistent with surface complexation modeling, which predicts a soluble As equilibrium concentration of 24 nM, which is of the same order of magnitude as the measured values at the end of the nitrate-amended experiments (around 10 nM).

Iron oxidation in the nitrate-amended microcosms ceases, even though significant levels of nitrate and HCl-extractable Fe(II) remain at the end of the experiments (Fig. 2A and 3). Possibly, the HCl extraction dissolves some Fe(II)-containing minerals that are unavailable to the Fe(II)-oxidizing bacteria. Alternatively, the encrustation by iron oxides of the Fe(II)-oxidizing organisms may cause their inactivation, a phenomenon that has been reported for enrichments of Fe(II)-oxidizing bacteria (13, 49). The exact reason for the apparent cessation of nitrate-dependent Fe(II) oxidation cannot be determined from our results. However, the slight increase in HCl-extracted Fe(II) observed after the second addition of nitrate (Fig. 3) may reflect the partial reduction of newly formed HFO, which provides an excellent electron acceptor for Fe(III)-reducing bacteria. Nonetheless, the partial reduction of HFO does not cause a release of As, likely because sufficient HFO surface sites remains to bind all the As.

The addition of nitrate caused a 300% increase in soluble Mn concentrations to more than 12 times the WHO guideline value of 7.3 μM (Fig. 1B). Human consumption of water with elevated Mn concentrations is hazardous and has been linked to mental deficiency in children (51). This release of Mn is clearly initiated by the addition of nitrate (non-nitrate-amended microcosms do not show this trend), but the mechanism of release cannot be determined with certainty from our data. However, there are several possibilities: (i) possible release of manganese as a result of cation exchange on the surfaces of clay minerals, possibly between H^+ and Mn^{2+}, since protons are produced during Fe(II) oxidation; (ii) microbial dissolution of Mn oxides, such as birnessite; and (iii) dissolution of carbonates, such as rhodocrosite.

Arsenic removal: sulfides. The sulfate-plus-lactate amendments also caused a dramatic decrease in soluble Fe and As (Fig. 1C), most probably driven by the production of sulfide associated with microbial sulfate reduction (21). The sulfate-plus-lactate amendments resulted in relative increases in the number of gene sequences from organisms related to the sulfate-reducing bacterium *Desulfovibrio puteali* (52) (Table 1). The observed increases in acetate (Fig. 2C) and propionate concentrations suggest a coupling of sulfate reduction to fermentation or incomplete lactate oxidation with sulfate. The production of measurable amounts of methane in these microcosms also indicates that some of these products fueled methanogenesis. Regardless of the mechanism, sulfate was rapidly removed from solution, presumably due to sulfate reduction. About 6.0 ± 1.7 mM sulfate was reduced within 52 days (Fig. 2B), while Eh simultaneously dropped to more reducing values. These changes were not observed in samples that were supplemented with sulfate plus lactate and then autoclaved (see Fig. S3 in the supplemental material).

The appearance of black color in the microcosms is characteristic of the formation of iron sulfide minerals. The reducing conditions indicated by an increase in Fe(II) seen in the Mössbauer spectra (see Fig. S4 in the supplemental material), the absence of free sulfide, and the decrease in soluble Fe(II) (Fig. 1C) are all consistent with the precipitation of FeS. However, the estimated maximum FeS concentration of 14 mmol (~1,200 ppm) represents ~2% of the total iron, too small to make a significant contribution to the Mössbauer spectra. Nevertheless, there is strong indirect evidence for the formation of FeS and the subsequent sorption of As. Given the formation of FeS in small quantities, the initial drop in the arsenic concentration detected within the first 13 days (Fig. 1C) likely reflects the sorption of As onto the surfaces of freshly formed FeS, for which arsenic has a high affinity (46, 53). Arsenic sorption is supported by the XANES and EXAFS spectra, which indicate As-S bonds consistent with As bound to the surface of FeS. The As-S bonding is preserved even after the sequential extraction. Assuming that As is sorbed exclusively to mackinawite, $FeS_{m(s)}$, and using the quantity of $FeS_{m(s)}$ calculated from the amount of sulfate reduced, an apparent partition coefficient, K_d, for As sorption to $FeS_{m(s)}$ of ~7 liters g^{-1} is obtained. This value agrees with the K_d range (2 to 9 liters g^{-1}) reported by Wolthers et al. (53), lending further support to removal of As by sorption to $FeS_{m(s)}$. Hence, there are several lines of evidence that support the formation of FeS and the sorption of As: (i) detection of sulfate-reducing bacteria only in samples treated with sulfate and lactate; (ii) biologically dependent sulfate consumption; (iii) absence of free sulfide, black color change, and a decrease in soluble Fe(II); (iv) XANES and EXAFS data that support As and S binding; and (v) a K_d of As sorption onto FeS within the range predicted by Wolthers et al. (53).

The final concentrations of aqueous As in the sulfate-plus-lactate treatments were significantly higher than in the nitrate treatments. Nonetheless, although the final soluble As concentrations (0.41 ± 0.13 μM) were well above the WHO threshold value, they were much lower than in the untreated microcosms. Similarly, studies on the *in situ* precipitation of As with sulfide (23) have shown that a partial removal of aqueous As in sediments can be achieved, but not to levels below the WHO guideline value, because As is less strongly bound to mackinawite than to Fe oxides. This is in line with the conclusions of Burton et al. (54), who showed that mackinawite formation during sulfidization of Fe

oxides is not a highly effective way to sequester As. It is, however, possible that prolonged sulfidogenesis in the microcosms could have allowed further As sequestration. Using the reaction path model (Fig. 4B) to predict the outcome of further sulfate reduction in the microcosms, it is predicted that extending the treatments would have resulted in more reducing conditions and higher sulfide concentrations. Under these conditions, the model predicts a predominance of soluble thioarsenic species and $FeS_{m(s)}$, which could lead to the formation of realgar-like surface precipitates on the surface of FeS (55) or of As sulfide mineral formation (56), thus sequestering As more efficiently.

Implications for arsenic remediation. The results of the nitrate and sulfate-plus-lactate amendments show that the activities of natural microbial populations present in aquifer sediments can be stimulated in order to immobilize arsenic. The microorganisms react quickly to the amendments, and soluble As removal is achieved over a time scale of weeks. During the initial decrease of soluble As, the two treatments yielded similar rates of removal at about 0.15 μmol As day^{-1}. However, the removal is more extensive when nitrate is supplied than for sulfate plus lactate. In the latter case, As levels are not brought into compliance with WHO guidelines within the duration of the experiments.

In Fig. 5 the predicted removal of soluble As along a flow path, under conditions representative of an aquifer of the type found in the area of Cambodia, where the samples for this study were collected, are compared for the two treatments. The simulations suggest that effective As remediation is achievable over a length scale of 50 m and within 6 months at the nitrate-dosing levels used in the nitrate-amended microcosms (Fig. 5A). It should be noted, however, that the dosing levels are an order of magnitude higher than the WHO nitrate groundwater concentration limit. At lower dosing levels, compliant with groundwater limits, it would take on the order of 3 years to achieve the same As removal. Clearly, dosing levels would need to be carefully considered in any remediation strategy. The remediation simulations further suggest that it would take over 4 years of sulfate-plus-lactate treatment to reach the final arsenic concentrations seen in the corresponding microcosms (Fig. 5B). Furthermore, those concentrations would still be well above the WHO guideline value. Lower aqueous As concentrations, below the WHO limit, were obtained by Saunders et al. (24) during an *in situ* treatment experiment in a Bangladeshi aquifer using injection of sulfate plus molasses. The reasons for the apparently contradictory results need further investigation.

Despite their potential usefulness in remediation, both treatments have significant drawbacks. As shown by our results, treatment with nitrate may exacerbate groundwater Mn contamination. Additional treatment would be needed before the groundwater could be used for domestic consumption, for example, by adding an aeration step for the extracted groundwater (57). Aeration could potentially remove any remaining soluble arsenic through sorption to the new Mn(IV) phases that would form. The use of sulfate plus lactate produces various fermentation products, most notably acetate and methane, which do not appear to be removed even when extra sulfate is added. Whereas these products themselves may not present a direct health threat, they are electron donors and could therefore affect redox processes in the subsurface in a variety of ways.

Because the attainment of groundwater As concentrations that meet WHO guidelines within a reasonable time frame should be the goal of any remediation method, our results suggest that inducing sulfate-reducing conditions alone would likely not be effective for the groundwater system from which the sediments were obtained. Treatment with nitrate would almost certainly be more effective and offers a possible treatment route, although additional measures may be needed to remove any undesired by-products that are released as a result of the addition of nitrate, most notably manganese.

ACKNOWLEDGMENTS

We thank David Cooke for the collection of the samples and RDI (Cambodia) for logistical support for this work. We also thank Alastair Bewsher, Catherine Davies, Paul Lythgoe, Paul Wincott, and Bart van Dongen for their help with laboratory work.

Funding for E.O.O. was provided by the European Commission Sixth Framework Marie Curie Actions project, AquaTRAIN, MRTN-CT-2006-035420. P.V.C. and R.-M.C. acknowledge financial support from the Canada Excellence Research Chair (CERC) Program.

The views expressed in the paper do not necessarily reflect those of the European Union or of any of the other funders.

REFERENCES

1. **Nordstrom DK.** 2002. Public health: worldwide occurrences of arsenic in ground water. Science **296:**2143–2145.
2. **Ravenscroft P, Brammer H, Richards K.** 2009. Arsenic pollution: a global synthesis. Wiley-Blackwell, Chichester, United Kingdom.
3. **Smith AH, Lopipero PA, Bates MN, Steinmaus CM.** 2002. Public health: arsenic epidemiology and drinking water standards. Science **296:**2145–2146.
4. **Smith AH, Lingas EO, Rahman M.** 2000. Contamination of drinking-water by arsenic in Bangladesh: a public health emergency. Bull. World Health Organ. **78:**1093–1103.
5. **WHO.** 2001. WHO environmental health criteria 224. Arsenic and arsenic compounds, 2001. World Health Organization. Geneva, Switzerland.
6. **Smedley PL, Kinniburgh DG.** 2002. A review of the source, behaviour and distribution of arsenic in natural waters. Appl. Geochem. **17:**517–568.
7. **Yu WH, Harvey CM, Harvey CF.** 2003. Arsenic in groundwater in Bangladesh: a geostatistical and epidemiological framework for evaluating health effects and potential remedies. Water Resour. Res. **39:**1146–1162.
8. **Islam FS, Gault AG, Boothman C, Polya DA, Charnock JM, Chatterjee D, Lloyd JR.** 2004. Role of metal-reducing bacteria in arsenic release from Bengal delta sediments. Nature **430:**68–71.
9. **Ainsworth CC, Pilon JL, Gassman PL, Vandersluys WG.** 1994. Cobalt, cadmium, and lead sorption to hydrous iron-oxide: residence time effect. Soil Sci. Soc. Am. J. **58:**1615–1623.
10. **Dixit S, Hering JG.** 2003. Comparison of arsenic(V) and arsenic(III) sorption onto iron oxide minerals: implications for arsenic mobility. Environ. Sci. Technol. **37:**4182–4189.
11. **Sun WJ, Sierra-Alvarez R, Milner L, Oremland R, Field JA.** 2009. Arsenite and ferrous iron oxidation linked to chemolithotrophic denitrification for the immobilization of arsenic in anoxic environments. Environ. Sci. Technol. **43:**6585–6591.
12. **Katsoyiannis IA, Zouboulis AI.** 2004. Application of biological processes for the removal of arsenic from groundwaters. Water Res. **38:**17–26.
13. **Straub KL, Benz M, Schink B, Widdel F.** 1996. Anaerobic, nitrate-dependent microbial oxidation of ferrous iron. Appl. Environ. Microbiol. **62:**1458–1460.
14. **Weber KA, Picardal FW, Roden EE.** 2001. Microbially catalyzed nitrate-dependent oxidation of biogenic solid-phase Fe(II) compounds. Environ. Sci. Technol. **35:**1644–1650.
15. **Straub KL, Buchholz-Cleven BEE.** 1998. Enumeration and detection of anaerobic ferrous iron-oxidizing, nitrate-reducing bacteria from diverse European sediments. Appl. Environ. Microbiol. **64:**4846–4856.
16. **Senn DB, Hemond HF.** 2002. Nitrate controls on iron and arsenic in an urban lake. Science **296:**2373–2376.
17. **Rowland H, Gault ALAG, Lythgoe P, Polya DA.** 2008. Geochemistry of aquifer sediments and arsenic-rich groundwaters from Kandal Province, Cambodia. Appl. Geochem. **23:**3029–3046.
18. **Buschmann J, Berg M.** 2009. Impact of sulfate reduction on the scale of arsenic contamination in groundwater of the Mekong, Bengal and Red River deltas. Appl. Geochem. **24:**1278–1286.
19. **Benner SG, Blowes DW, Ptacek CJ.** 1997. A full-scale porous reactive

wall for prevention of acid mine drainage. Ground Water Monit. Remediat. **17:**99–107.
20. **Dvorak DH, Hedin RS, Edenborn HM, McIntire PE.** 1992. Treatment of metal contaminated water using bacterial sulfate reduction—results from pilot scale reactors. Biotechnol. Bioeng. **40:**609–616.
21. **Rabus R, Hansen TA, Widdel F.** 2006. Dissimilatory sulfate- and sulfur-reducing prokaryotes, p 659–768. *In* Dworkin M, Falkow S, Rosenberg E, Schleifer K-H, Stackebrandt E (ed), The prokaryotes. Springer, New York, NY.
22. **Kirk MF, Holm TR, Park J, Jin QS, Sanford RA, Fouke BW, Bethke CM.** 2004. Bacterial sulfate reduction limits natural arsenic contamination in groundwater. Geology **32:**953–956.
23. **Kirk MF, Roden EE, Crossey LJ, Brearley AJ, Spilde MN.** 2010. Experimental analysis of arsenic precipitation during microbial sulfate and iron reduction in model aquifer sediment reactors. Geochim. Cosmochim. Acta **74:**2538–2555.
24. **Saunders JA, Lee MK, Shamsudduha M, Dhakal P, Uddin A, Chowdury MT, Ahmed KM.** 2008. Geochemistry and mineralogy of arsenic in (natural) anaerobic groundwaters. Appl. Geochem. **23:**3205–3214.
25. **Polizzotto ML, Kocar BD, Benner SG, Sampson M, Fendorf S.** 2008. Near-surface wetland sediments as a source of arsenic release to ground water in Asia. Nature **454:**505–508.
26. **Berg M, Stengel C, Trang PTK, Viet PH, Sampson ML, Leng M, Samreth S, Fredericks D.** 2007. Magnitude of arsenic pollution in the Mekong and Red River Deltas: Cambodia and Vietnam. Sci. Total Environ. **372:**413–425.
27. **Lovley DR, Phillips EJ.** 1986. Organic matter mineralization with reduction of ferric iron in anaerobic sediments. Appl. Environ. Microbiol. **51:**683–689.
28. **Smieja JA, Wilkin RT.** 2003. Preservation of sulfidic waters containing dissolved As(III). J. Environ. Monit. **5:**913–916.
29. **Niemann H, Duarte J, Hensen C, Omoregie E, Magalhaes VH, Elvert M, Pinheiro LM, Kopf A, Boetius A.** 2006. Microbial methane turnover at mud volcanoes of the Gulf of Cadiz. Geochim. Cosmochim. Acta **70:**5336.
30. **Ludwig W, Strunk O, Westram R, Richter L, Meier H, Yadhukumar Buchner A, Lai T, Steppi S, Jobb G, Forster W, Brettske I, Gerber S, Ginhart AW, Gross O, Grumann S, Hermann S, Jost R, Konig A, Liss T, Lussmann R, May M, Nonhoff B, Reichel B, Strehlow R, Stamatakis A, Stuckmann N, Vilbig A, Lenke M, Ludwig T, Bode A, Schleifer K-H.** 2004. ARB: a software environment for sequence data. Nucleic Acids Res. **32:**1363–1371.
31. **Pruesse E, Quast C, Knittel K, Fuchs BM, Ludwig WG, Peplies J, Glockner FO.** 2007. SILVA: a comprehensive online resource for quality checked and aligned ribosomal RNA sequence data compatible with ARB. Nucleic Acids Res. **35:**7188–7196.
32. **Nordstrom DK, Archer DG.** 2003. Arsenic thermodynamic data and environmental geochemistry, p 2–25. *In* Welch AH, Stollenwerk KG (ed), Arsenic in groundwater. Kluwer, Boston, MA.
33. **Couture RM, Gobeil C, Tessier A.** 2010. Arsenic, iron and sulfur codiagenesis in lake sediments. Geochim. Cosmochim. Acta **74:**1238–1255.
34. **Helz GR, Tossell JA.** 2008. Thermodynamic model for arsenic speciation in sulfidic waters: a novel use of ab initio computations. Geochim. Cosmochim. Acta **72:**4457–4468.
35. **Rowland H, Pederick ALRL, Polya DA, Pancost RD, Van Dongen BE, Gault AG, Vaughan DJ, Bryant C, Anderson B, Lloyd JR.** 2007. The control of organic matter on microbially mediated iron reduction and arsenic release in shallow alluvial aquifers, Cambodia. Geobiology **5:**281–292.
36. **Lovley D.** 2006. Dissimilatory Fe(III)- and Mn(IV)-reducing prokaryotes, p 635–658. *In* Dworkin M, Falkow S, Rosenberg E, Schleifer K-H, Stackebrandt E (ed), The prokaryotes. Springer, New York, NY.
37. **Lloyd JR, Gault AG, Héry M, MacRae JD.** 2011. Microbial transformations of arsenic in the subsurface, p 77–90. *In* Stolz JF, Oremland RS (ed), Environmental microbe-metal intereactions II. ASM Press, Washington, DC.
38. **MacRae JD, Lavine IN, McCaffery KA, Ricupero K.** 2007. Isolation and characterization of NP4, arsenate-reducing Sulfurospirillum, from Maine groundwater. J. Environ. Eng. **133:**81–88.
39. **Stolz JF, Oremland RS.** 1999. Bacterial respiration of arsenic and selenium. FEMS Microbiol. Rev. **23:**615–627.
40. **Coker VS, Gault A, Pearce GC, van der Laan IG, Telling ND, Charnock J, Polya MDA, Lloyd JR.** 2006. Incorporation of As(V) within biogenic nano-magnetite: a study using X-ray circular dichroism and X-ray absorption spectroscopy. Environ. Sci. Technol. **40:**7745–7750.
41. **Weiss JV, Rentz JA, Plaia T, Neubauer SC, Merrill-Floyd M, Lilburn T, Bradburne C, Megonigal JP, Emerson D.** 2007. Characterization of neutrophilic Fe(II)-oxidizing bacteria isolated from the rhizosphere of wetland plants and description of Ferritrophicum radicicola gen. nov. sp. nov., and Sideroxydans paludicola sp. nov. Geomicrobiol. J. **24:**559–570.
42. **Emerson D, Moyer C.** 1997. Isolation and characterization of novel iron-oxidizing bacteria that grow at circumneutral pH. Appl. Environ. Microbiol. **63:**4784–4792.
43. **Rickard D.** 2006. The solubility of FeS. Geochim. Cosmochim. Acta **70:**5779–5789.
44. **Couture R-M, Van Cappellen P.** 2011. Reassessing the role of sulfur geochemistry on arsenic speciation in reducing environments. J. Hazard. Mater. **189:**647–652.
45. **Wolthers M, Charlet L, Van der Weijden CH, Van der Linde PR, Rickard D.** 2005. Arsenic mobility in the ambient sulfidic environment: sorption of arsenic(V) and arsenic(III) onto disordered mackinawite. Geochim. Cosmochim. Acta **69:**3483–3492.
46. **Farquhar ML, Charnock JM, Livens FR, Vaughan DJ.** 2002. Mechanisms of arsenic uptake from aqueous solution by interaction with goethite, lepidocrocite, mackinawite, and pyrite: an X-ray absorption spectroscopy study. Environ. Sci. Technol. **36:**1757–1762.
47. **Lear G, Song B, Gault AG, Polya DA, Lloyd JR.** 2007. Molecular analysis of arsenate-reducing bacteria within Cambodian sediments following amendment with acetate. Appl. Environ. Microbiol. **73:**1041–1048.
48. **van Dongen BE, Rowland H, Gault ALAG, Polya DA, Bryant C, Pancost RD.** 2008. Hopane, sterane and n-alkane distributions in shallow sediments hosting high arsenic groundwaters in Cambodia. Appl. Geochem. **23:**3047–3058.
49. **Blothe M, Roden EE.** 2009. Composition and activity of an autotrophic Fe(II)-oxidizing, nitrate-reducing enrichment culture. Appl. Environ. Microbiol. **75:**6937–6940.
50. **Waychunas GA, Rea BA, Fuller CC, Davis JA.** 1993. Surface chemistry of ferrihydrite. 1. EXAFS studies of the geometry of coprecipitated and adsorbed arsenate. Geochim. Cosmochim. Acta **57:**2251–2269.
51. **Wasserman GA, Liu XH, Parvez F, Ahsan H, Levy D, Factor-Litvak P, Kline J, van Geen A, Slavkovich V, Lolacono NJ, Cheng ZQ, Zheng Y, Graziano JH.** 2006. Water manganese exposure and children's intellectual function in Araihazar, Bangladesh. Environ. Health Perspect. **114:**124–129.
52. **Basso O, Caumette P, Magot M.** 2005. *Desulfovibrio putealis* sp. nov., a novel sulfate-reducing bacterium isolated from a deep subsurface aquifer. Int. J. Syst. Evol. Microbiol. **55:**101–104.
53. **Wolthers M, Butler IB, Rickard D, Mason PRD.** 2005. Arsenic uptake by pyrite at ambient environmental conditions: a continuous-flow experiment. Am. Chem. Soc. Symp. Ser. **915:**60–76.
54. **Burton ED, Johnston SG, Bush RT.** 2011. Microbial sulfidogenesis in ferrihydrite-rich environments: effects on iron mineralogy and arsenic mobility. Geochim. Cosmochim. Acta **75:**3073–3087.
55. **Gallegos TJ, Hyun SP, Hayes KF.** 2007. Spectroscopic investigation of the uptake of arsenite from solution by synthetic mackinawite. Environ. Sci. Technol. **41:**7781–7786.
56. **O'Day PA, Vlassopoulos D, Root R, Rivera N.** 2004. The influence of sulfur and iron on dissolved arsenic concentrations in the shallow subsurface under changing redox conditions. Proc. Natl. Acad. Sci. U. S. A. **101:**13703–13708.
57. **Hallberg KB, Johnson DB.** 2005. Biological manganese removal from acid mine drainage in constructed wetlands and prototype bioreactors. Sci. Total Environ. **338:**115–124.